

Turbulence in virtual Origin of the variance and skewness of density function

Xunchuan Liu (刘训川)^{1,2}

¹ Leiden Observatory, Leiden University, P.O. Box 9513, 2300RA Leiden, The Netherlands
e-mail: liuxunchuan001@gmail.com

² Shanghai Astronomical Observatory, Chinese Academy of Sciences, 80 Nandan Road, Shanghai 200030, PR China

Draft Feb 2025

ABSTRACT

Turbulence is a complex phenomenon that plays a critical role in the interstellar medium (ISM). Previous simulations and observations show that the probability density function (PDF) of gas density in isothermal and compressible systems under turbulence exhibits a near lognormal shape, with a strong empirical relation between the variance (σ^2) and Mach number (\mathcal{M}). In this work, we aim to explain the σ^2 - \mathcal{M} relation and the deviation from the lognormal shape from a thermodynamic and cascading perspective. By introducing a virtual dissipation process, during which turbulent entropy and structural dissipation are assumed to be coupled, we derive the empirical relation $\sigma^2 = \ln(1 + \mathcal{M})^2$. Additionally, by introducing a delay parameter q for the local gas temperature, we derive the deviation from the empirical relation at high \mathcal{M} . We further argue that the exponential tails of PDFs (on the $s = \ln(\rho)$ scale) arise from the convolution of PDF kernels, which can be skewed at both the low- s and high- s ends. Skewness has limited influence on the σ^2 - \mathcal{M} relation. Two density-fraction strategies – the mass-fraction and volume-fraction approaches – are introduced to explain the physical origins of the low- s and high- s skewed PDF kernels. These two types of PDF kernels are dual to each other and exhibit highly symmetric mathematical structures. We speculate that the high- s skewed PDF kernels are physical and may be analogous to the high-density tails of column-density PDFs in molecular clouds, which are influenced by gravity. Inspired by this, we propose a form of an ‘isothermal’ turbulent system that likely favors the volume-fraction strategy.

Key words. Turbulence — ISM: kinematics and dynamics — ISM: clouds

1. Introduction

Turbulence is a ubiquitous phenomenon in fluid dynamics (Kolmogorov 1941; Burgers 1948). It is also crucial to understanding a wide range of astrophysical and interstellar processes. Turbulence, along with gravity and possibly magnetic fields, is believed to govern the behavior of gas in molecular clouds (e.g., Orkisz et al. 2017), star-forming regions (e.g., Liu et al. 2025b), and many other astrophysical systems (e.g., Veltri 1999; Read et al. 2020; Paneque-Carreño et al. 2024), where it plays a pivotal role in regulating energy, momentum, and mass transport (e.g., Larson 1981; McKee & Tan 2003). The origin of interstellar turbulence is still not fully understood and may be related to the large-scale structure of the interstellar medium (ISM), which is highly turbulent and driven by a combination of forces, e.g., shear force (e.g., Miyamoto et al. 2014), stellar feedback (e.g., Carroll et al. 2009; Gent 2012), cloud-cloud collisions (e.g., Wu et al. 2018), and instability under gravity (e.g., Goldbaum et al. 2015).

A key feature of turbulent flows in these systems is the probability density function (PDF) of gas density (ρ), which has been found to follow a lognormal distribution in simulations (Vazquez-Semadeni 1994; Padoan et al. 1997; Federrath et al. 2010). In observations, due to the projection effect, only column density can be obtained, which also follows a lognormal distribution in gravity-non-dominated regions (Berkhuijsen & Fletcher 2008; Schneider et al. 2015; Liu et al. 2025a). The variance of the lognormal distribution, often denoted as σ^2 , is known, based on simulations, to depend on the Mach number \mathcal{M} ,

which measures the velocity fluctuations relative to the sound speed (Padoan et al. 1997; Federrath et al. 2010; Konstandin et al. 2012; Hopkins 2013). Observations of various types of ISM systems, such as diffuse atomic clouds (Liu et al. 2025a) and denser molecular clouds (e.g., Goodman et al. 2009; Burkhardt et al. 2015), also support the σ^2 - \mathcal{M} . This relation is thus very likely fundamental to understanding the behavior of turbulence in compressible and isothermal gas systems.

However, despite the empirical success of finding the σ^2 - \mathcal{M} in simulations and its broad application in observations, a comprehensive physical theoretical explanation of this relationship remains absent. While the k - ϵ turbulence model (Lauder & Spalding 1979; Pittard et al. 2009) has been successful in predicting empirical results in many turbulent systems, it does not provide a theoretical framework for explaining the σ^2 - \mathcal{M} relation of isothermal and compressible systems, which are typically the cases for astronomical objects such as the ISM (Goldsmith 2001; Heiles & Troland 2003; Hopkins 2013; Yue et al. 2021). Providing a self-consistent theory to explain the σ^2 - \mathcal{M} relation for both subsonic and supersonic systems, as well as compressive and solenoidal driving forces (Federrath et al. 2010; Konstandin et al. 2012), and the deviation from the empirical relation in supersonic systems (Federrath et al. 2008; Hopkins 2013), within the same framework, is particularly important in gas dynamics and astrophysical contexts.

Besides, simulations also show that for supersonic systems (with Mach number $\mathcal{M} > 1$), especially those driven by compressive forcing, the PDFs are lognormal at the high-density end

but tend to skew toward the low-density (and low $s = \ln(\rho)$) end (e.g., [Federrath et al. 2010](#)). Such a low- s skewed lognormal PDF has also been observed in the HI 21 cm line emission of a very high-velocity cloud, observed with the FAST 500-m telescope ([Liu et al. 2025a](#)). The physical origin of the skewness in the PDFs of turbulent systems (referred to as the skewness of turbulence) remains an open question. [Hopkins \(2013\)](#), interpreting turbulence as a cascading process that broadens the PDF through convolution at successive cascade levels ([Kolmogorov 1941](#); [Castaing 1996](#); [Yakhot 1998](#)), speculated that the low- s skewness arises from PDF convolution kernels due to intermittency. However, they did not explicitly demonstrate how intermittency generates exponential tails from physical principles. Beyond the lack of a physical explanation for turbulence skewness, there is another intrinsic motivation for exploring the PDF skewness: Is it correlated with the $\sigma^2 - \mathcal{M}$ relation? That is, we aim to present a theory explaining the origins of the two key parameters of the density PDFs in isothermal and compressible systems under turbulence: the variance (σ^2) and skewness (τ , as will be seen in this work).

In this work, we provide a concise thermodynamic and cascading perspective on turbulence, offering a theoretical framework for understanding the $\sigma^2 - \mathcal{M}$ relation and PDF skewness in turbulent systems with different Mach numbers and driving forces. In Sect. 2, we introduce background knowledge and definitions related to the probability density functions (PDFs) of gas density on the $s = \ln(\rho)$ scale. In Sect. 3, we focus on the underlying processes of turbulent and structural dissipation, deriving the empirical $\sigma^2 - \mathcal{M}$ relation and its deviations under appropriate assumptions. In Sect. 4, we describe two density-fraction strategies to explain the origins of PDF kernels skewed at both ends. We also introduce the concept of a ‘dual’ operation to characterize the highly symmetric structure between the PDF kernels resulting from these two strategies. In Sect. 5, we present further discussions, including: the influence of skewness on the $\sigma^2 - \mathcal{M}$ relation (Sect. 5.1); the physical interpretation of high- s skewed kernels by exploring the mathematical construction of corresponding turbulent systems (Sect. 5.2); and considerations and limitations of this work (Sect. 5.3). Finally, we provide a brief summary in Sect. 6.

2. Background knowledge and basic definitions

In this work, we use PDF to represent the PDF of ρ or s , with no ambiguity. A normalized PDF (on the logarithmic scale $s = \ln(\rho)$), denoted as $f(s)$, should satisfy the following two conditions:

$$\int f ds = 1, \quad (1)$$

$$\int f e^s ds = 1. \quad (2)$$

Here, we have rescaled the density unit to ensure that $\langle \rho \rangle = 1$.

Let g and h be two normalized PDFs, and $f * g$ their convolution, it can be shown that:

$$\begin{aligned} \int (g * h)(s) e^s ds &= \int g(s-t) h(t) e^s dt ds \\ &= \int h(t) e^t dt = 1. \end{aligned} \quad (3)$$

Thus, $g * h$ is also a normalized PDF. Let $\sigma^2(g)$ denote the variance of g . Then, the variance of $g * h$ satisfies

$$\sigma^2(g * h) = \sigma^2(g) + \sigma^2(h). \quad (4)$$

If we further assume that $g \propto e^{ax}$ and $h \propto e^{bx}$ for $x < 0$, with $a > b > 0$, then:

$$g * h \propto \int e^{ay} e^{b(x-y)} dy \propto e^{bx} \quad \text{for } x \rightarrow -\infty. \quad (5)$$

Therefore, convolution cannot introduce the exponential tail of the convolution kernels. The resulting convolved curve will have an exponential index equal to that of the convolution kernel with the flattest tail.

Simulations from the 1990s ([Vazquez-Semadeni 1994](#); [Padoan et al. 1997](#)) found that the PDFs of the gas density (ρ) in isothermal and compressible systems due to turbulence follow lognormal distributions, in the form of

$$f_{\text{normal}}(s) = \frac{1}{\sqrt{2\pi}\sigma} \exp\left(-\frac{(s + \sigma^2/2)^2}{2\sigma^2}\right). \quad (6)$$

The mean ($-\sigma^2/2$) and variance (σ^2) of P are correlated to ensure Eq. 2.

3. PDF variance from a thermodynamic perspective

3.1. Empirical $\sigma^2 - \mathcal{M}$ relation

The variance of Eq. 6 is σ^2 , with its value depending on the Mach number (\mathcal{M}), and can be estimated from (e.g., [Padoan et al. 1997](#)).

$$\sigma^2 \sim \ln(1 + b^2 \mathcal{M}^2). \quad (7)$$

For compressive forcing, $b = 1$ ([Federrath et al. 2010](#)). For solenoidal forcing, [Federrath et al. \(2010\)](#) suggested a value of $b = \frac{1}{3}$, and [Konstandin et al. \(2012\)](#) interpreted it as the ratio of the Mach number of the compressive motion ($\mathcal{M}_{\text{comp}}$) to the total Mach number. In the subsonic regime, the solenoidal driving force may lead to b being much lower than $\frac{1}{3}$ ([Konstandin et al. 2012](#)).

Note that for \mathcal{M} much lower than 1, the compressive motion can be treated as a sound wave, which would lead to

$$\frac{\langle |\delta\rho| \rangle}{\langle \rho \rangle} = \frac{\langle |\delta V| \rangle}{V_s} = \mathcal{M}_{\text{comp}}, \quad (8)$$

where V is the velocity field and V_s is the speed of sound. The solenoidal motion, if it exists in the form of quasi-steady rotating eddies, will contribute to density enhancement through centrifugal force:

$$|\delta\rho| \sim \frac{1}{V_s^2} \frac{\rho V^2}{R} \sim \mathcal{M}^2 \rho \ll \mathcal{M} \rho. \quad (9)$$

The compressive motion can be quickly radiated away (depending on the boundary conditions), leading to a very low ratio of $\mathcal{M}_{\text{comp}}/\mathcal{M}$, and thus to a very small value of b . Below, by default, we treat \mathcal{M} as $\mathcal{M}_{\text{comp}}$ and $b = 1$ in Eq. 7.

3.2. $\sigma^2 - \mathcal{M}$ relation by entropy coupling

Here, we attempt to understand the turbulent system from the perspective of thermodynamics. Note that N particles have $3N$ degrees of freedom, the same as in Fourier k -space. The compressive mode has N degrees of freedom, one for each particle on average. We assume, as suggestions by simulations ([Federrath et al. 2010](#)), that only the compressive modes will be excited during the dissipation of the velocity field established by

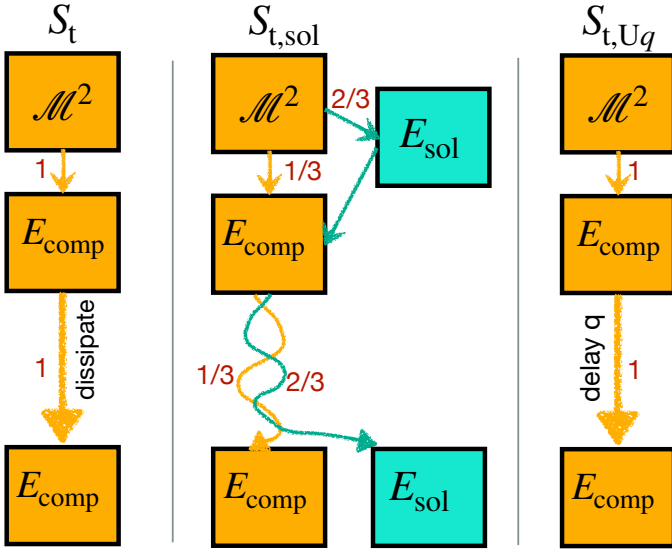


Fig. 1. Sketch maps for three different scenarios illustrating how we calculate the increase in entropy due to turbulent energy dissipation (from top to bottom). E_{comp} and E_{sol} represent the energy carried by the compressive and solenoidal velocity components, respectively. See Sect. 3 for details (Eqs. 13, 19, and 23). For $S_{t,\text{sol}}$, we consider the 3D case here. The red number represents the ratio of energy passing through each route.

compressive forcing (see the case of solenoidal forcing in Sect. 3.3).

We consider a virtual process: the injection of turbulent energy suddenly ceases, and the turbulent energy dissipates in an adiabatic and quasi-static manner, down to compressive modes below the dissipation scale. The temperature of the high- k compressive modes will increase from thermal temperature T_{thermal} to T_{final} with

$$T_{\text{final}} = T_{\text{thermal}} + T_{\text{turb}}. \quad (10)$$

Here,

$$T_{\text{turb}} = \mathcal{M}^2 T_{\text{thermal}}. \quad (11)$$

Due to turbulent dissipation, the entropy of the system will increase by

$$S_t \propto \int_{T_{\text{thermal}}}^{T_{\text{final}}} \frac{1}{T} dT \quad (12)$$

$$= \ln\left(\frac{T_{\text{final}}}{T_{\text{thermal}}}\right) \quad (13)$$

$$= \ln(1 + \mathcal{M}^2).$$

Here, we have omitted the constant factors for the particle number and the Boltzmann constant, k_B .

The entropy contributed by the density structure, described by a given probability density function (PDF) denoted as f , is given by

$$S_s \propto -2 \int \rho \ln(\rho) dV \quad (14)$$

$$= -2 \int f(\rho) \rho \ln(\rho) d\rho$$

$$= -2 \int f(s) s e^s ds$$

For a lognormal distribution (Eq. 6), it can be verified that

$$S_s(f_{\text{normal}}) = -2 \int \frac{1}{\sqrt{2\pi}\sigma} \exp\left(-\frac{(s + \sigma^2/2)^2}{2\sigma^2}\right) s e^s ds$$

$$= -2 \int \frac{1}{\sqrt{2\pi}\sigma} \exp\left(-\frac{(s - \sigma^2/2)^2}{2\sigma^2}\right) s ds$$

$$= -2E(f_{\text{normal}}(-s)) = 2E(f_{\text{normal}}(s))$$

$$= -\sigma^2. \quad (15)$$

Here, $E(f)$ denotes the mean of f . A more compact proof is provided in Eq. 69. Note that the factor of 2 in Eq. 14 is introduced to normalize Eq. 15. During the dissipation process described above, the entropy increase due to structural dissipation is $|S_t|$. Note that, by equating Eqs. 13 and 15, that is, by setting

$$|S_t| = |S_s|, \quad (16)$$

we immediately obtain a $\sigma^2 - \mathcal{M}$ relation identical to that in Eq. 7 with $b = 1$.

We thus propose that, during the dissipation process, the increase in entropy associated with turbulent dissipation (Eq. 13) should be coupled with that of the structural dissipation (Eq. 15), providing a constraint on the relation between σ and \mathcal{M} . Note that, in astronomical objects such as molecular clouds, the system typically maintains a constant temperature, balanced by cooling and heating mechanisms (Bergin & Tafalla 2007). The above constraint remains valid in such cases, since turbulence, once fully established, transports its energy from large scales to smaller scales in a cascading manner, with most of the energy dissipated at the smallest scale (dissipation scale; Kolmogorov 1941). The turbulence “feels” little difference between the heating processes (adiabatic or isothermal) occurring at the smallest dissipation scale.

3.3. The case of solenoidal forcing

For solenoidal forcing in a D -dimensional system, solenoidal turbulent motion is injected at large scales, and compressive motion is subsequently induced during energy cascading. In k space, the ratio between the degree of freedom of the compressive mode and that of the entire k space is given by $1/D$. Assuming that under solenoidal forcing, the solenoidal motion acts as an energy pool, $1/D$ of the turbulent energy resides in the intermediate k space, where both solenoidal and compressive modes are fully excited (see Fig. 1). Thus, we can write:

$$T_{\text{final}} = T_{\text{thermal}} + \left(\frac{\mathcal{M}}{D}\right)^2 T_{\text{thermal}} = T_{\text{thermal}} + \mathcal{M}_{\text{comp}}^2 T_{\text{thermal}}, \quad (17)$$

where

$$\mathcal{M}_{\text{comp}} = \frac{1}{D} \mathcal{M}. \quad (18)$$

Therefore, we have:

$$S_{t,\text{sol}} = \ln\left(1 + \mathcal{M}_{\text{comp}}^2\right). \quad (19)$$

It provides an explanation of why $b = \frac{1}{D}$ for a pure solenoidal driving force (e.g., Federrath et al. 2010). In the $\sigma^2 - \mathcal{M}$ relation (Eq. 7), \mathcal{M} should be interpreted as $\mathcal{M}_{\text{comp}}$, regardless of how it is generated, whether directly by compressive forcing or secondarily induced by solenoidal forcing. If $\mathcal{M}_{\text{comp}}$ is adopted, we should take $b = 1$.

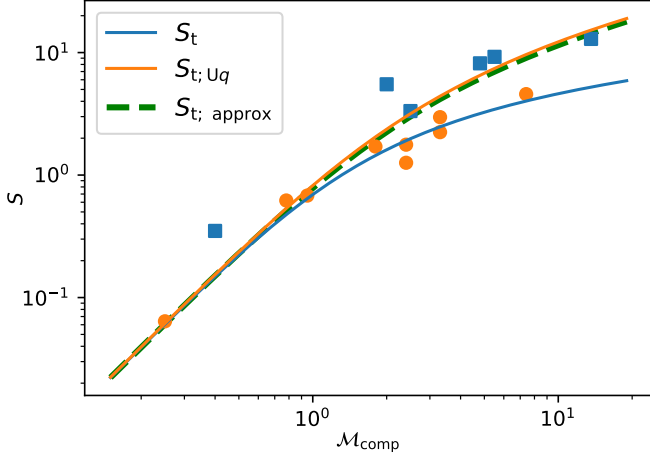


Fig. 2. Comparison of the different forms of S_t in Eqs. 13, 23, and 26 (Sect. 3). The markers represent simulations results (only including those not magnetically dominated) tabulated by Hopkins (2013) (see also references therein). The yellow circles and blue squares denote simulations with solenoidal and compressive forcing schemes, respectively. The x -axis represents the Mach number of the compressive component of the turbulent velocity field (M_{comp}).

3.4. Deviation from the $\sigma^2 - M$ relation

In Sect. 3.2, to derive Eq. 13, we virtually introduce an adiabatic and quasi-static process of dissipation. This assumption may not be entirely accurate, particularly for turbulence driving by compressive forcing with a high M , where some of the large-scale turbulent energy may bypass the cascading process and be directly dissipated. To sustain the turbulent velocity field, a higher energy input rate at the large scale is required compared to the fully cascading process. Thus, a σ^2 greater than the value given by Eq. 7 (or equivalently Eq. 15) is expected for supersonic turbulence, as indicated by simulations from around 2010 (Federath et al. 2008; Schmidt et al. 2009; Federrath et al. 2010; Konstandin et al. 2012; Molina et al. 2012).

For each high- k mode, the inner energy will eventually increase from T_{thermal} to T_{final} . Denote ΔT as the energy a high- k mode receives from turbulence before a given time. At that time, its temperature (T) is not necessarily $T_{\text{thermal}} + \Delta T$, due to the coupling of structural dissipation. Instead, we introduce a delay parameter (q) to describe the increase of local temperature, which modifies Eq. 12 as

$$S_{t; q} = \int_0^{T_{\text{turb}}} \frac{1}{(T_{\text{thermal}} + qT)} dT \quad (20)$$

$$= \frac{1}{q} \ln(1 + qM^2). \quad (21)$$

We further assume that q is a variable uniformly distributed between 0 and 1, reflecting the stochastic nature of turbulence, that is

$$q \sim U(0, 1). \quad (22)$$

It leads to

$$S_{t; Uq} = \int_0^1 S_{t; q} dq \quad (23)$$

$$= \int_0^1 \frac{1}{q} \ln(1 + qM^2) dq \quad (24)$$

$$= -\text{Li}_2(-M^2). \quad (24)$$

Here, Li_2 denotes the dilogarithm function. Eq. 23 is exactly the empirical form of σ^2 suggested by Hopkins (2013), obtained by fitting the simulation data¹. Note that

$$S_{t; Uq} \sim \begin{cases} S_t \sim M^2 \sim [\ln(1 + M)]^2 & \text{for } M \ll 1 \\ 2[\ln(1 + M)]^2 & \text{for } M \gg 1. \end{cases} \quad (25)$$

Thus, we suggest using the following formula to approximate $S_{t; Uq}$, or equivalently, $-\text{Li}_2(-M^2)$:

$$S_{t; Uq} \sim S_{t; \text{approx}} = (2 - e^{-M})[\ln(1 + M)]^2. \quad (26)$$

$S_{t; \text{approx}}$ deviates from $S_{t; Uq}$ by less than six percent, providing a good approximation. See Fig. 2 for the comparison between S_t , $S_{t; Uq}$, and $S_{t; \text{approx}}$. Overall, from the thermodynamic perspective, we derive that the PDFs of a turbulent system driven by compressive forcing should have

$$\sigma^2 = S_{t; Uq} = -\text{Li}_2(-M^2). \quad (27)$$

This is consistent with simulations (Fig. 2).

4. PDF Skewness and fraction strategies

4.1. PDF skewness at both ends

4.1.1. PDF kernels of low- s skewness by H13

Hopkins (2013), having noticed the special role of the exponential PDF kernels (Eq. 5), successfully fitted the low- s -skewed PDFs. One of the key ideas of the H13 model is to construct the PDF by repeatedly convolving a low- s -end skewed kernel on the logarithmic scale. The form of the kernel they chosen is

$$f_\tau(s) = A \exp\left(-\frac{s_{\text{cut}} - s}{\tau}\right) (s < s_{\text{cut}}). \quad (28)$$

To make f_τ normalized,

$$s_{\text{cut}} = \ln(1 + \tau), \quad (29)$$

$$A = \frac{1}{\tau}. \quad (30)$$

A PDF with the exponential tail of f_τ and a dispersion σ_0 can be constructed through repeatedly convolved f_τ by λ times with (Hopkins 2013):

$$\lambda = \frac{\sigma_0^2}{\tau^2}. \quad (31)$$

The resultant PDF, $f_{\tau; \lambda}$, is (Hopkins 2013):

$$f_{\tau; \lambda}(s) = (f_\tau)^{* \lambda}(s) \quad (32)$$

$$= \frac{1}{\Gamma(\lambda)} \frac{1}{\tau} \left(\frac{\lambda \ln(1 + \tau) - s}{\tau} \right)^{\lambda-1} \exp\left(-\frac{|s - \lambda \ln(1 + \tau)|}{\tau}\right).$$

with $f_{\tau; \lambda}(s) = 0$ for $s > \lambda \ln(1 + \tau)$. Here, $f^{* \lambda}$ denotes the successive convolution of λ instances of f . To implement this convolution process with non-integer λ , Hopkins (2013) treated it as a variable following a Poisson distribution with a mean of σ_0^2/τ^2 .

¹ The integral $\int_0^1 \frac{1}{q} \ln(1 + qx) dq = \int_0^x \frac{1}{q} \ln(1 + q) dq$ (Eq. 23) is not equal to $\text{Li}_2(x)$, as suggested by Hopkins (2013), but to $-\text{Li}_2(-x)$. Note that, $\text{Li}_2(x) \equiv \sum_{n=1}^{\infty} \frac{x^n}{n^2}$.

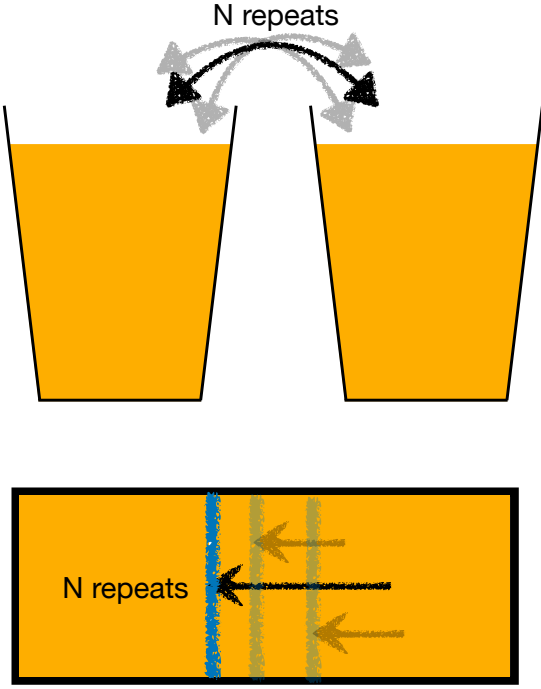


Fig. 3. Sketch map of density fraction strategies: Mass fraction (top) and volume fraction (bottom) strategies (Sect. 4). Among the N virtual realizations of the processes, the one that creates the smallest difference between the two subvolumes is realized.

4.1.2. PDF kernels of high- s skewness

In Eq. 28, $f_\tau(s)$ is presumed to skew to the low- s end. However, under physical effects such as gravity, it may skew to the high- s end. Similarly, we can define a high- s -skewed f_τ^+ as:

$$f_\tau^+(s) = A^+ \exp\left(-\frac{s - s_{\text{cut}}^+}{\tau}\right) \quad (s > s_{\text{cut}}^+), \quad (33)$$

where,

$$s_{\text{cut}}^+ = \ln(1 - \tau), \quad (34)$$

$$A^+ = \frac{1}{\tau}. \quad (35)$$

Unlike the low- s -skewed case, here, τ must be smaller than 1 to ensure mass conservation. $f_{\tau,n}^+$ can be constructed in the same manner as $f_{\tau,n}$ (Sect. 4.1.1).

f_τ and f_τ^+ are not just symmetric in mathematical form. In the following sections, we will provide a physical explanation of f_τ and f_τ^+ , along with their modified forms, demonstrating that they are actually linked to two kinds of fraction strategies. Moreover, the high- s -skewed PDF kernel may not be as unphysical as it initially appears.

Similar to the velocity cascading process in turbulence, the density of compressive gas in a turbulent system is also expected to develop in a cascading and self-similar manner. Below, we propose two strategies for the density fraction process of a single step in detail and present the explicit forms of their corresponding PDF kernels (on the logarithmic scale).

4.2. Skewness via different density fraction strategies?

4.2.1. Mass fraction and low- s skewed PDF kernels

Here, we consider two buckets of equal unit volume, each containing a unit mass (upper panel of Fig. 3). In a single mass

exchange process, the buckets randomly exchange a mass δm , where δm follows a uniform distribution between -1 and 1 . This is why we refer to it as the mass-fraction strategy. It can be shown that the distribution of the mass within one bucket (or the density) follows $f_{\tau=1}$.

Now, we consider that in each step, there are virtually N independent repetitions of such mass exchange processes. Based on the principle of least action, the mass exchange process that minimizes the mass difference (i.e., the one with the smallest $|\delta m|$) is the one actually executed in that step. Note that the total mass is conserved. As a result, one of the two buckets will have a density smaller than 1, while the other will have a density greater than 1. For the bucket with the lower density, the probability that its density is less than ρ (where $\rho < 1$) is given by

$$\text{CDF}_{N,Mf}(\rho) = \frac{1}{2}\rho^N. \quad (36)$$

Thus, the PDFs of ρ and s for that bucket are

$$f_{N,Mf}(\rho) = \frac{d \text{CDF}_{N,Mf}}{d\rho} = \frac{N}{2}\rho^{N-1}, \quad (37)$$

$$f_{N,Mf}(s) = P_{N,Mf}(\rho) \frac{d\rho}{ds} = \frac{N}{2}\rho^N = \frac{N}{2}e^{Ns}. \quad (38)$$

Comparison between Eqs. 38 and 28 yields $\tau = 1/N$. For the bucket with $\rho > 1$, due to mass conservation, the PDFs are given by

$$f_{N,Mf}(\rho) = P_{N,Mf}(2 - \rho) = \frac{N}{2}(2 - \rho)^{N-1}, \quad (39)$$

$$f_{N,Mf}(s) = \frac{N}{2}(2 - e^s)^{N-1}e^s. \quad (40)$$

We thus suggest a modified form of f_τ :

$$f_{\tau,\text{modif}} = \begin{cases} \frac{1}{2\tau}e^{s/\tau} & \text{for } s \leq 0, \\ \frac{1}{2\tau}(2 - e^s)^{\frac{1-\tau}{\tau}}e^s & \text{for } 0 < s < \ln(2). \end{cases} \quad (41)$$

The procedure outlined above ensures that $f_{\tau,\text{modif}}$ is a normalized PDF, satisfying Eqs. 1 and 2.

The upper panel of Fig. 4 shows a comparison between f_τ and $f_{\tau,\text{modif}}$. For small τ (or equivalently small N), $f_{\tau,\text{modif}}$ tends to be more symmetric, implying that $f_{\tau,\text{modif}}$ may be more physically realistic than f_τ . However, a small τ typically corresponds to the case of low \mathcal{M} , where the PDF kernels are repeatedly convolved multiple times, ultimately approaching a Gaussian-like PDF. In this scenario, there is little difference between the different convolution kernels. In Fig. 5, we compare $(f_{\tau,\text{modif}})^{*n}$ and $f_{\tau,\lambda}$ (Sect. 4.1.1) with the same τ and σ^2 . They are similar to each other, especially at the low- s end where skewness occurs. Note that for small τ , the variance $\sigma^2(f_{\tau,\text{modif}})$ is no longer τ^2 , as is the case for f_τ . Instead, we have (Fig. 6)

$$\sigma^2(f_{\tau,\text{modif}}) \sim 2\tau^2, \quad \text{as } \tau \rightarrow 0. \quad (42)$$

A drawback of the modified kernel is that to construct a PDF with a variance of σ^2 through convolution from $f_{\tau,\text{modif}}$, the repetitions of the kernels cannot simply be given by σ^2/τ^2 .

For the super-extreme case of $f_{\tau,\text{modif}}$ with $\tau \rightarrow \infty$, $N = 1/\tau \rightarrow 0$, although N cannot be an integer, the equations from Eq. 36 to Eq. 41 remain valid mathematically. Let $\tau \rightarrow \infty$, we have

$$f_{\tau \rightarrow \infty; \text{modif}} = \begin{cases} \sim \frac{1}{2\tau} & \text{for } -\tau < s \leq 0, \\ \sim \frac{1}{2\tau} \frac{e^s}{2 - e^s} & \text{for } 0 < s \leq \ln(2 - e^{-\tau}). \end{cases} \quad (43)$$

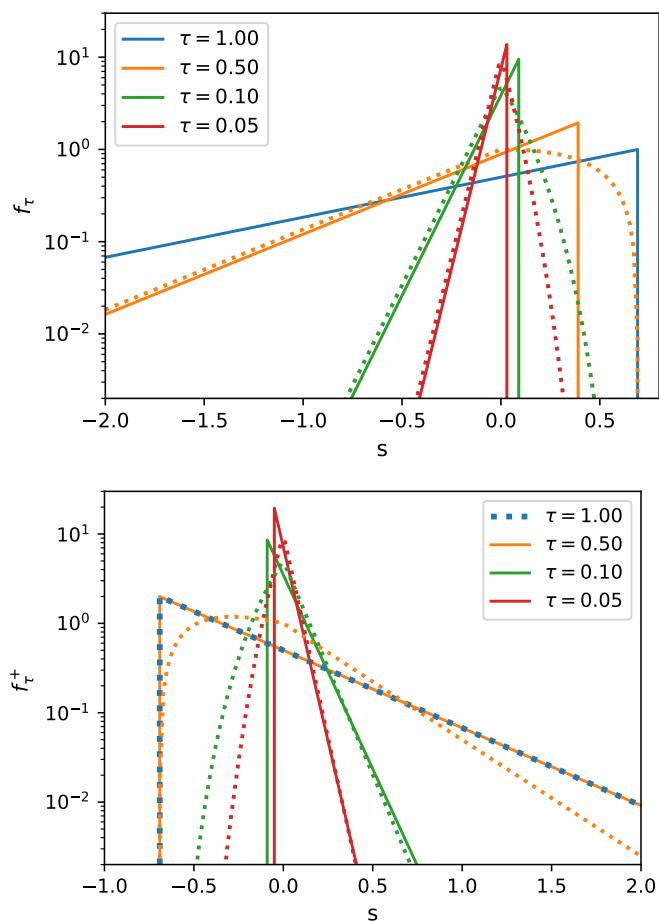


Fig. 4. Upper: The black solid lines show f_τ for different values of τ (Eq. 28). Dotted lines represent $f_{\tau,\text{modif}}$, the modification of f_τ suggested by Eq. 41. Lower: Same as the upper panel but for f_τ^+ (solid) and $f_{\tau,\text{modif}}^+$ (dotted) (see Eqs. 33 and 53). Note that for $\tau = 1$, f_τ^+ is undefined.

There is another form of the above equation:

$$f_{\tau \rightarrow \infty; \text{modif}} \sim \begin{cases} \frac{1}{2\tau} & \text{for } -\tau < s < \ln(2 - e^{-\tau}), \quad (44) \\ \frac{1}{2} \text{Dirac}(\ln(2)) & \text{for } s = \ln(2). \quad (45) \end{cases}$$

Here, Dirac represents the Dirac delta function. Note that the mass integral ($\int e^s f ds$) of Eq. 44 converges to 0 as $\tau \rightarrow \infty$, while the integral of Eq. 45 is 1. In this context,

$$f_{\tau \rightarrow \infty; \text{modif}} \sim \text{Dirac}(\ln(2)). \quad (46)$$

4.2.2. Volume fraction and high- s skewed PDF kernels

The mass-fraction strategy described above maintains the volumes of the buckets while exchanging the mass they contain. This motivates the consideration of another strategy in which the mass is not exchanged, but the volumes of the buckets are altered. We refer to this strategy as the volume-fraction strategy (Fig. 3).

In the volume-fraction strategy, we consider a slab that divides a large volume ($\mathcal{V}_{\text{tot}} = 2$) into two buckets, each containing a mass of 2 (Fig. 3). In a single volume exchange process, the slab is randomly moved, resulting in a volume difference ($\delta\mathcal{V}$) between the two buckets, which follows a uniform distribution

between -1 and 1 . Similar to the mass-fraction strategy, we now consider that in each step, there are virtually N independent repetitions of such volume exchange processes, and the volume exchange process that minimizes the volume difference is the one actually executed in that step. Then, for the bucket with $s > 0$ (or equivalently $\mathcal{V} < 1$), we have

$$\text{CDF}_{N,V_f}(\mathcal{V}) = \frac{1}{2} \mathcal{V}^N, \quad (47)$$

$$f_{N,V_f}(\mathcal{V}) = \frac{N}{2} \frac{1}{\mathcal{V}^{N+1}}, \quad (48)$$

$$f_{N,V_f}(s) = \frac{N}{2} e^{-Ns}. \quad (49)$$

Again, a comparison between Eqs. 49 and 33 leads to $\tau = 1/N$. For the bucket with $\rho < 1$, due to volume conservation, the PDF can be written as

$$f_{N,V_f}(s) = \frac{N}{2} (2 - e^{-s})^{N-1} e^{-s}. \quad (50)$$

It seems to suggest that the modified form of f_τ^+ is

$$f_{\tau; \text{modif}; \dagger}^+ = \begin{cases} \frac{1}{2\tau} e^{-s/\tau} & \text{for } s \geq 0, \\ \frac{1}{2\tau} (2 - e^{-s})^{\frac{1-\tau}{\tau}} e^{-s} & \text{for } \ln\left(\frac{1}{2}\right) < s < 0. \end{cases} \quad (51)$$

with good symmetry with $f_{\tau,\text{modif}}(-s)$:

$$f_{\tau; \text{modif}; \dagger}^+(s) \equiv f_{\tau,\text{modif}}(-s). \quad (52)$$

However, $f_{\tau; \text{modif}; \dagger}^+$ is not a normalized PDF; it satisfies Eq. 1 but not Eq. 2. The key point is that the PDF discussed in this work is a volume-weighted statistic. In the volume fraction strategy, a weight proportional to $\mathcal{V} = 1/\rho = e^{-s}$ must be taken into account. Thus, we adopt a modified form of f_τ^+ (Fig. 4):

$$f_{\tau; \text{modif}}^+(s) = e^{-s} f_{\tau; \text{modif}; \dagger}^+ = e^{-s} f_{\tau,\text{modif}}(-s). \quad (53)$$

It can be verified that $f_{\tau; \text{modif}}^+$ satisfies both Eqs. 1 and 2. This is not a coincidence; for further discussion, see Sect. 4.3. The simple mathematical form of Eq. 53 suggests that the two density-fraction strategies are, in some sense, symmetric to each other.

As in Eqs. 44 and 45, we have

$$f_{\tau \rightarrow \infty; \text{modif}}^+ \sim \begin{cases} \frac{e^{-s}}{2\tau} & \text{for } \ln(e^{-\tau} - 2) < s < \tau, \quad (54) \\ \text{Dirac}(-\ln(2)) & \text{for } s = -\ln(2). \quad (55) \end{cases}$$

Unlike in Eq. 46, here we cannot omit Eq. 54, because its mass integral is non-zero:

$$\int_0^\tau \frac{e^{-s}}{2\tau} e^s ds = \frac{1}{2}. \quad (56)$$

Thus, half of the mass of the system will contribute to the high- s exponential tail of Eq. 54.

4.3. Duality between the two fraction strategies

In this section, we demonstrate that the low- s -skew PDFs and high- s -skew PDFs are 'dual' to each other. This confirms, from a mathematical standpoint, the speculation that the two density-fraction strategies (Sect. 4) are fundamental and orthogonal strategies, and thus may both occur in turbulent systems, under specific conditions.

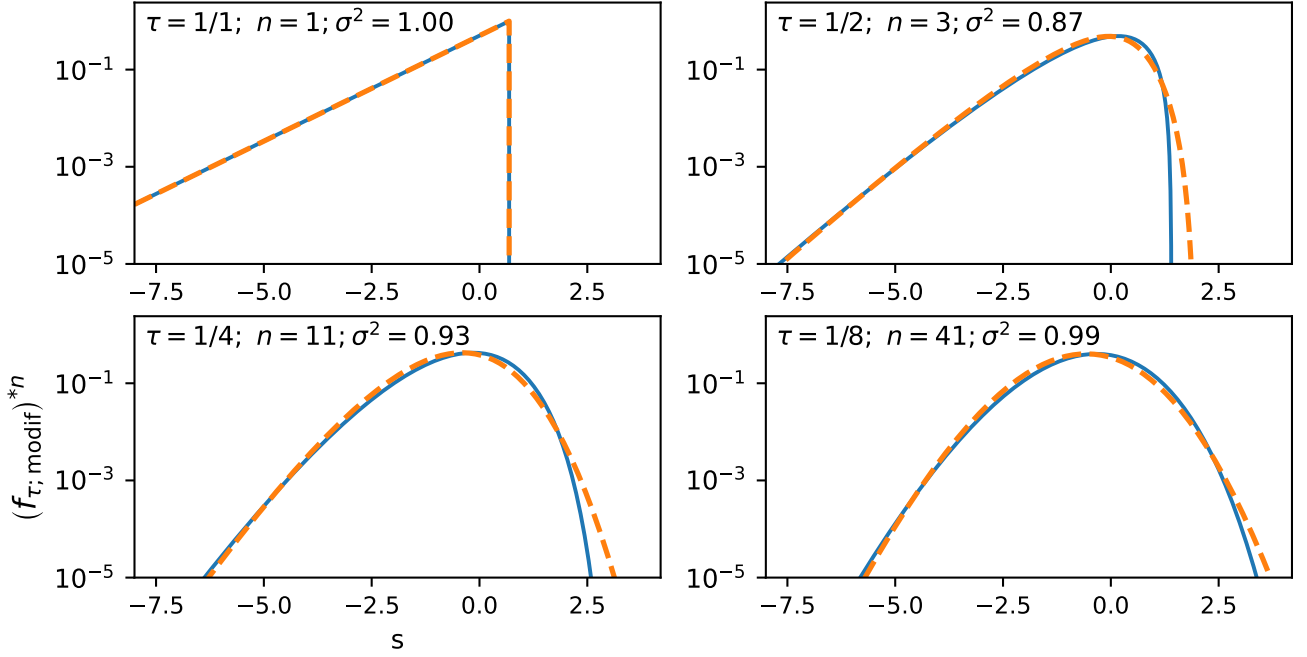


Fig. 5. In each panel, the yellow dashed line represents $(f_{\tau; \text{modif}})^{*n}$, the result of the successive convolution of n instances of $(f_{\tau; \text{modif}})$. The parameters τ and n , as well as the σ^2 of $(f_{\tau; \text{modif}})^{*n}$, are labeled in the upper left corner. The blue solid line corresponds to $f_{\tau; \lambda}$ with a τ identical to that of $f_{\tau; \text{modif}}$, and $\lambda = \sigma^2/\tau^2$, ensuring that $(f_{\tau; \text{modif}})^{*n}$ and $f_{\tau; \lambda}$ have the same σ^2 . Note that for $\tau = 1$ and $n = 1$, the two curves overlap because, in this case, there is no modification (Sect. 4.2.1).

Let $f(s)$ be any normalized PDF that satisfies both Eqs. 1 and 2, and denote the dual of f as

$$f^{\text{dual}}(s) \equiv \text{Dual}[f](s) = e^{-s} f(-s). \quad (57)$$

Then, we have:

$$\int f^{\text{dual}}(s) ds = \int e^{-s} f(-s) ds = \int e^s f(s) ds = 1, \quad (58)$$

$$\int e^s f^{\text{dual}}(s) ds = \int f(-s) ds = \int f(s) ds = 1. \quad (59)$$

So, P^{dual} is also a normalized PDF, and

$$\text{Dual}[f^{\text{dual}}](s) \equiv f(s). \quad (60)$$

From the above equations, it can be easily proved that $f_{\tau; \text{modif}}^+$ (Eq. 52) is a normalized PDF, since $f_{\tau; \text{modif}}^+ = \text{Dual}[f_{\tau; \text{modif}}]$.

We define a space of purely low- s -skewed PDFs, denoted \mathcal{F}_L , as follows:

1. For any $\tau > 0$, $f_{\tau; \text{modif}} \in \mathcal{F}_L$;
2. For any integer $n > 1$ and $f_{\tau_i} \in \mathcal{F}_L$ for $i = 1, \dots, n$, the convolution $f_{\tau_1} * f_{\tau_2} * \dots * f_{\tau_n} \in \mathcal{F}_L$.
3. For any f and g in \mathcal{F}_L and $0 \leq t \leq 1$, $tf + (1-t)g \in \mathcal{F}_L$.

Any $f \in \mathcal{F}_L$ has an exponential tail (as $s \rightarrow -\infty$) with an exponential factor of $1/\min(\tau_i)$. Similarly, we can define a space of purely high- s -skewed PDFs, denoted \mathcal{F}_H from $f_{\tau; \text{modif}}^+$.

Note that the operations of dual and convolution are exchangeable:

$$\begin{aligned} f^{\text{dual}}(s) * g^{\text{dual}}(s) &= [f(-s)e^{-s}] * [g(-s)e^{-s}] \\ &= [f(-s) * g(-s)] \cdot e^{-s} \\ &= f * g(-s) \cdot e^{-s} \\ &= (f * g)^{\text{dual}}(s), \end{aligned} \quad (61)$$

Also, we have

$$af^{\text{dual}} + bg^{\text{dual}} = (af + bg)^{\text{dual}}. \quad (62)$$

It follows that

$$\text{Dual}[f] \in \mathcal{F}_H \quad \text{for } f \in \mathcal{F}_L, \quad (63)$$

$$\text{Dual}[f] \in \mathcal{F}_L \quad \text{for } f \in \mathcal{F}_H. \quad (64)$$

\mathcal{F}_L and \mathcal{F}_H are dual to each other:

$$\text{Dual}[\mathcal{F}_L] = \mathcal{F}_H, \quad \text{Dual}[\mathcal{F}_H] = \mathcal{F}_L. \quad (65)$$

Similarly, we define a space \mathcal{F} of skewed PDFs generated from $f_{\tau; \text{modif}}$ and $f_{\tau; \text{modif}}^+$. We have

$$\text{Dual}[\mathcal{F}] = \mathcal{F}. \quad (66)$$

Any $f \in \mathcal{F}$ can be uniquely decomposed as the convolution of two PDFs: one in \mathcal{F}_L and one in \mathcal{F}_H . Pure Gaussian PDFs (Eq. 6) can be viewed as special cases of skewed PDFs and approximated by Gaussian-like functions $f \in \mathcal{F}$. Note that,

$$\text{Dual}[f_{\text{normal}}] = f_{\text{normal}}. \quad (67)$$

5. Discussion

5.1. Influence of skewness on $\sigma^2 - \mathcal{M}$ relation

In Sect. 3.2, we demonstrate that the fundamental relation for structural entropy,

$$S_s(f) = -2 \int f s e^s ds = -\sigma^2(f), \quad (68)$$

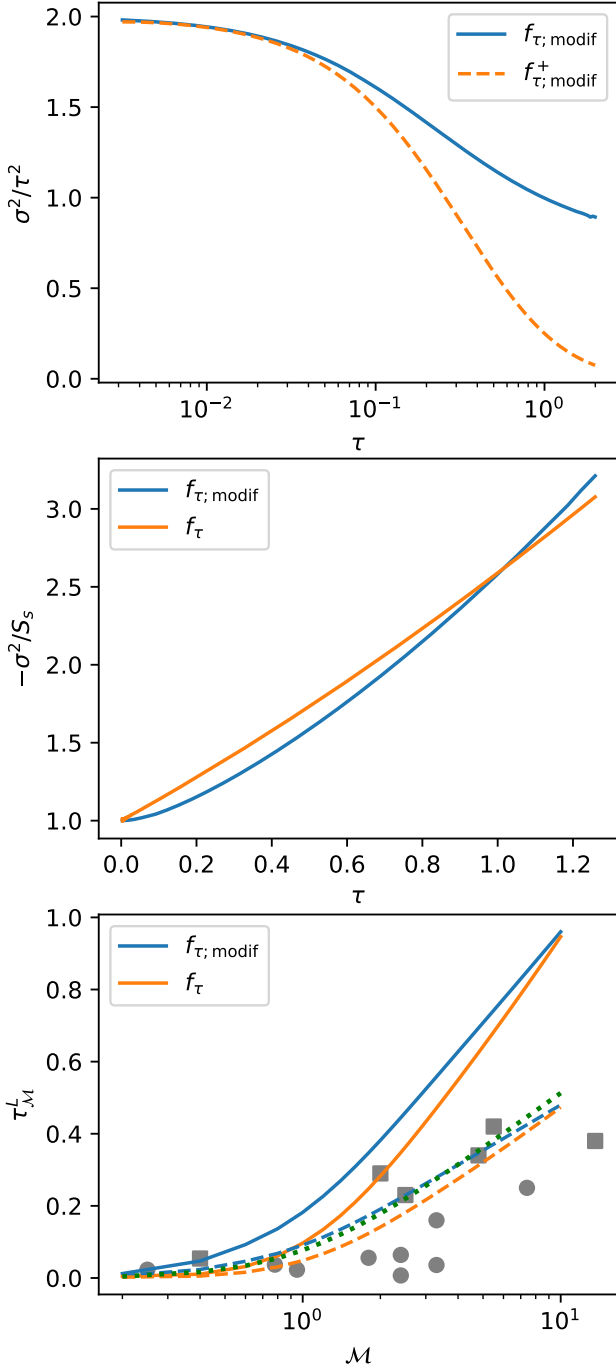


Fig. 6. Upper: The ratio of the variance of the kernels to τ^2 , for $f_{\tau, \text{modif}}$ (blue) and $f_{\tau, \text{modif}}^+$ (orange). Middle: The ratio between the variance (σ^2) and the structural entropy (S_s) of the kernels. Lower: The solid lines show the curves of τ_M^L (see Sect. 5.1 for details). The dashed lines are the solid lines divided by a factor of 2. The green dotted line is $\ln(1 + \mathcal{M}^2)/9$. The gray squares and circles show the τ of $f_{\tau, \lambda}$ fitted by Hopkins (2013), based on simulations driven by compressive and solenoidal forcing, respectively.

holds for a Gaussian-like PDF (f_{normal}). A more concise proof follows from Eq. 67:

$$\begin{aligned} S_s(f_{\text{normal}}) &= -2 \int f_{\text{normal}}(s) s e^s ds = 2 \int f_{\text{normal}}(-s) s e^{-s} ds \\ &= 2 \int \text{Dual}[f_{\text{normal}}] s ds = 2 \int f_{\text{normal}} s ds \\ &= 2E(f_{\text{normal}}) = -\sigma^2. \end{aligned} \quad (69)$$

Next, we examine whether the skewed PDF kernels of f_{τ} and $f_{\tau, \text{modif}}$ also satisfy this relation (Eq. 68).

For f_{τ} , $\sigma^2(f_{\tau}) = \tau^2$. When τ is small (see the middle panel of Fig. 6),

$$S_s(f_{\tau}) \sim \tau^2 = \sigma^2 \quad \text{as } \tau \rightarrow 0. \quad (70)$$

However, the ratio of σ^2/S_s grows as τ increases.

For $f_{\tau, \text{modif}}$ with $N = 1/\tau \gg 1$, the value of S_s is²

$$\begin{aligned} S_s(f_{\tau, \text{modif}}) &= - \int_0^1 N \rho^N \ln(\rho) d\rho - \int_1^2 N(2-\rho)^{N-1} \rho \ln(\rho) d\rho \\ &= \frac{N}{(N+1)^2} - \int_0^1 N \rho^{N-1} (2-\rho) \ln(2-\rho) d\rho \\ &\sim \tau \left(\frac{1}{1+2\tau} - \left(\frac{2}{1+\tau} - \frac{1}{1+3\tau} \right) (1-\tau) \right) \\ &\sim -2\tau^2 \sim -\sigma^2(f_{\tau, \text{modif}}). \end{aligned} \quad (71)$$

However, the ratio of σ^2/S_s also increases with τ . The σ^2/S_s for f_{τ} and $f_{\tau, \text{modif}}$ are similar to each other (Fig. 6).

In Sect. 3.4, we propose a delay parameter q to explain the deviation of the PDF variance from the empirical $\sigma^2 - \mathcal{M}$ relation for turbulent systems driven by compressive forcing. Here, we denote the deviation factor as (Eqs. 13 and 24)

$$X(\mathcal{M}) = \frac{S_t; Uq}{S_t}, \quad (72)$$

and \mathcal{M} should be interpreted as the Mach number of the compressive velocity component ($\mathcal{M}_{\text{comp}}$; see Sect. 3.3). If such a deviation is fully due to the skewness of the kernel (f_{τ} or $f_{\tau, \text{modif}}$), then we should get a lower limit of τ as

$$\tau_M^L = \text{solve} \left(-\frac{\sigma^2(f_{\tau})}{S_s(f_{\tau})} = X(\mathcal{M}), \tau \right). \quad (73)$$

Here, τ_M^L is the lower limit because the PDF would approach a lognormal distribution after convolution, and thus the ratio $\frac{\sigma^2}{S_s}$ will approach 1. The curve of τ_M^L along \mathcal{M} is shown in the bottom panel of Fig. 6, for both f_{τ} and $f_{\tau, \text{modif}}$. The τ values, obtained by fitting the simulated PDFs using $f_{\tau, \lambda}$ as done by Hopkins (2013), are also shown. The fitted τ values are all smaller than τ_M^L . We thus conclude that the PDF skewness cannot fully explain the deviation of the $\sigma^2 - \mathcal{M}$ relation.

An auxiliary result can be obtained from the dashed and dotted lines in the bottom panel of Fig. 6. For turbulent systems with compressive forcing, the following equation may serve as a rough estimation of the $\tau - \mathcal{M}$ relation:

$$\tau_M = 0.5\tau_M^L \sim \frac{1}{\mathcal{D}^2} \ln(1 + \mathcal{M}^2), \quad (74)$$

with $\mathcal{D} = 3$ the dimension of the system. We do not know if such a relation still holds for 2D systems. For turbulent systems driven by solenoidal forcing, τ_M is even lower (Fig. 6). We thus suggest that PDF skewness (τ) and variance are two relevant, but not fully dependent, statistical parameters of turbulent systems.

² Note that $\int_1^2 x^N \ln(x) dx = \frac{{}_2F_1(1, 2+N, 3+N, 1/2)}{2(1+N)(2+N)}$.

5.2. High- s skewed systems

The low- s and high- s skewed PDF kernels, derived from two different density fraction strategies, are dual to each other with a highly symmetric mathematical structure. Thus, it is very likely that the high- s -skewed PDF kernel is physical. Molecular clouds, which can be treated as isothermal systems governed by both turbulence and gravity, usually show high-density-end power-law tails (on the ρ scale; corresponding to exponential tails on the s scale) on their PDFs of column densities (e.g., Schneider et al. 2013; Brunt 2015; Alves et al. 2017; Zhang et al. 2025). Simulations also confirm this phenomenon (e.g., Veltchev et al. 2024). We speculate that it may be related to the high- s -skewed PDF kernels promoted in this work. Initiated by this idea, we try to construct turbulent systems that biases toward high- s skewed PDFs.

The Mach number plays a critical role in turbulence, so the isothermal feature should be at least partly maintained. The momentum equation of isothermal gas fluid is

$$\frac{\partial \mathbf{v}}{\partial t} + (\mathbf{v} \cdot \nabla) \mathbf{v} = -\frac{1}{\rho} \nabla P - \Delta \phi, \quad (75)$$

with

$$P = \rho c_s^2 = \rho T_{\text{thermal}}. \quad (76)$$

Here, c_s is the sound speed, and $c_s^2 = T_{\text{thermal}}$ ignoring constant terms. In a turbulence-gravity coupling system, a gravity-bound region that is suddenly compressed by turbulence will typically provide positive pressure due to its density-enhanced boundary. However, as the density structure adjusts under the influence of gravity, that region may provide weak or even no pressure to counteract the external pressure. Thus, analogously, we construct a system that does not contain the $\Delta \phi$ term, and instead has a modified pressure term:

$$P = \rho T \cdot \mathcal{L}(\mathcal{D}, \det(\mathcal{H})). \quad (77)$$

Here, \mathcal{L} is a function of $\mathcal{D} = \nabla(\rho \mathbf{v})$, \mathcal{H} is the Hessian matrix of the density (taken with respect to space), and $\det(\mathcal{H})$ is the determinant of \mathcal{H} . The simplest form of \mathcal{L} is

$$\mathcal{L}(x, y) = \begin{cases} 1 - \Omega & \text{for } x > 0, y < 0, \\ 1 & \text{otherwise.} \end{cases} \quad (78)$$

That is, when the gas is locally compressed, the pressure term works normally (Eq. 76). When the density-enhanced region is expanding, the pressure term is reduced. If $\Omega = 0$, the system reverts to the normal state. If $\Omega = 1$, a velocity convergent region will increase its density and never return to its previous state. This is the essence of the volume-fraction strategy. We thus speculate that, within this framework, Ω describes the weight of the volume-fraction strategy. Under the influence of gravity, the molecular cloud (in regions above a certain threshold) behaves similarly, leading to high- s skewed PDFs, provided the density-enhanced region has not yet globally collapsed under gravity. A detailed investigation of the system's behavior (Eq. 78) and its connection to the skewness of PDFs will be left for future exploration.

5.3. Considerations and limitations

Several important considerations should be noted in this work. In Sect. 5.2, we discuss the possibility of constructing a system that favors the volume-fraction strategy. It is important to note

that this approach differs from the Burgers model for a totally pressureless gas (Burgers 1948). Even for $\Omega = 1$, the system described in Sect. 5.2 will not lead to density divergence because the pressure term persists during compression. However, at this stage, this remains a conceptual construction. Future simulations may help us explore the density structures of such systems and provide further insights into their behavior and evolution.

Another important consideration of this work deserving notation is that, at present, we have not taken magnetic fields (B-field) into account. Magnetic fields can significantly influence turbulence, especially in the ISM. Extending this perspective to include magnetohydrodynamics (MHD) could provide a more comprehensive understanding of turbulent flows; however, it introduces some challenges. When the magnetic field is extremely strong, the gas system may reduce to a two-dimensional (2D) system, where certain dynamics are constrained. In the presence of a mild magnetic field, it becomes difficult to consider the roles of Alfvén waves, fast waves, and slow waves, which exhibit different wave speeds (e.g., Beresnyak & Lazarian 2019). The fast wave plays a role analogous to the sound speed; however, slow waves exhibit a more complex coupling between the density structure and the velocity field. It is important to note that a steady gas system with over-dense regions confined by the magnetic field gradient can be treated as a special case of slow waves. Thus, we are uncertain whether the entropy increase due to turbulent dissipation and structural dissipation is still coupled to each other in a simple relation, as we assumed for hydrodynamic systems.

6. Summary

In this work, we present a thermodynamic and cascading theory to explain the origins of the variance and skewness of the density (on the $s = \ln(\rho)$ scale) PDFs for isothermal compressible gas under turbulence. The main results include:

1. We obtain the empirical relation $\sigma^2 = \ln(1 + \mathcal{M}^2)$ by introducing a virtual dissipation process, during which entropy increases due to structural dissipation, with turbulence dissipation assumed to be coupled. Further, we introduce a delay parameter for the local gas temperature and quantitatively derive the deviation from the empirical $\sigma^2 - \mathcal{M}$ relation, which describes both subsonic and supersonic turbulence in the same framework.
2. We found that the PDF kernels with low- s skewed exponential tails can be explained by the virtual density fraction through a so-called mass-fraction strategy. Similarly, the high- s skewed kernels can be explained by a so-called volume-fraction strategy.
3. The explicit forms of the PDF kernels are derived. The two types of PDF kernels, produced by different strategies, exhibit highly symmetric structures. We introduce the concept of ‘duality’ to describe the relationship between the spaces of high- s -skewed and low- s -skewed PDFs.
4. Skewness has limited influence on the $\sigma^2 - \mathcal{M}$ relation. We suggest that PDF skewness (τ) and variance are two relevant, but not fully dependent, statistical parameters of turbulent systems.
5. We speculate that the high-density power-law tails of the column density PDFs of molecular clouds may be related to the high- s -skewed PDF kernels. Inspired by this, we briefly describe a form of turbulent system that may prefer the volume-fraction strategy.

Overall, this work presents a framework for understanding the statistical properties of the density PDFs of turbulent gas systems. While the results offer some insight, further investigations and simulations will be needed to fully explore the complexities of turbulence and its density structures, as well as the potential role of magnetic fields, which remain unexplored here.

Acknowledgements. X. Liu acknowledges the support of the Strategic Priority Research Program of the Chinese Academy of Sciences under Grant No. XDB0800303, and the National Key R&D Program of China under Grant No. 2022YFA1603100. X. Liu also thanks the Leiden University for providing working space of this work.

References

- Alves, J., Lombardi, M., & Lada, C. J. 2017, *A&A*, 606, L2
- Beresnyak, A. & Lazarian, A. 2019, *Turbulence in Magnetohydrodynamics* (Berlin, Boston: De Gruyter)
- Bergin, E. A. & Tafalla, M. 2007, *ARA&A*, 45, 339
- Berkhuijsen, E. M. & Fletcher, A. 2008, *MNRAS*, 390, L19
- Brunt, C. M. 2015, *MNRAS*, 449, 4465
- Burgers, J. M. 1948, in *Advances in Applied Mechanics*, ed. R. V. Mises & T. V. Kármán, Vol. 1 (Elsevier), 171–199
- Burkhart, B., Lee, M.-Y., Murray, C. E., & Stanimirović, S. 2015, *ApJ*, 811, L28
- Carroll, J. J., Frank, A., Blackman, E. G., Cunningham, A. J., & Quillen, A. C. 2009, *ApJ*, 695, 1376
- Castaing, B. 1996, *Journal de Physique II*, 6, 105
- Federrath, C., Klessen, R. S., & Schmidt, W. 2008, *ApJ*, 688, L79
- Federrath, C., Roman-Duval, J., Klessen, R. S., Schmidt, W., & Mac Low, M. M. 2010, *A&A*, 512, A81
- Gent, F. A. 2012, PhD thesis, Newcastle University Upon Tyne, UK
- Goldbaum, N. J., Krumholz, M. R., & Forbes, J. C. 2015, *ApJ*, 814, 131
- Goldsmith, P. F. 2001, *ApJ*, 557, 736
- Goodman, A. A., Pineda, J. E., & Schnee, S. L. 2009, *ApJ*, 692, 91
- Heiles, C. & Troland, T. H. 2003, *ApJ*, 586, 1067
- Hopkins, P. F. 2013, *MNRAS*, 430, 1880
- Kolmogorov, A. 1941, *Akademiia Nauk SSSR Doklady*, 30, 301
- Konstantin, L., Girichidis, P., Federrath, C., & Klessen, R. S. 2012, *ApJ*, 761, 149
- Larson, R. B. 1981, *Monthly Notices of the Royal Astronomical Society*, 194, 809
- Launder, B. & Spalding, D. 1979, *Lectures in Mathematical Models of Turbulence* (Academic Press)
- Liu, X., Liu, T., Li, P.-S., et al. 2025a, arXiv e-prints, arXiv:2502.10897
- Liu, X., Liu, T., Mai, X., et al. 2025b, arXiv e-prints, arXiv:2501.17502
- McKee, C. F. & Tan, J. C. 2003, *ApJ*, 585, 850
- Miyamoto, Y., Nakai, N., & Kuno, N. 2014, *PASJ*, 66, 36
- Molina, F. Z., Glover, S. C. O., Federrath, C., & Klessen, R. S. 2012, *MNRAS*, 423, 2680
- Orkisz, J. H., Pety, J., Gerin, M., et al. 2017, *A&A*, 599, A99
- Padoan, P., Nordlund, A., & Jones, B. J. T. 1997, *MNRAS*, 288, 145
- Paneque-Carreño, T., Izquierdo, A. F., Teague, R., et al. 2024, *A&A*, 684, A174
- Pittard, J. M., Falle, S. A. E. G., Hartquist, T. W., & Dyson, J. E. 2009, *MNRAS*, 394, 1351
- Read, P. L., Young, R. M. B., & Kennedy, D. 2020, *Geoscience Letters*, 7, 10
- Schmidt, W., Federrath, C., Hupp, M., Kern, S., & Niemeyer, J. C. 2009, *A&A*, 494, 127
- Schneider, N., André, P., Könyves, V., et al. 2013, *ApJ*, 766, L17
- Schneider, N., Ossenkopf, V., Csengeri, T., et al. 2015, *A&A*, 575, A79
- Vazquez-Semadeni, E. 1994, *ApJ*, 423, 681
- Veltchev, T. V., Girichidis, P., Marinkova, L., et al. 2024, *MNRAS*, 528, 432
- Veltri, P. 1999, *Plasma Physics and Controlled Fusion*, 41, A787
- Wu, B., Tan, J. C., Nakamura, F., Christie, D., & Li, Q. 2018, *PASJ*, 70, S57
- Yakhov, V. 1998, *Phys. Rev. E*, 57, 1737
- Yue, N.-N., Li, D., Zhang, Q.-Z., et al. 2021, *Research in Astronomy and Astrophysics*, 21, 024
- Zhang, C., Liu, T., Jiao, S., et al. 2025, arXiv e-prints, arXiv:2501.16682